P-204L: *Late-News Poster:* Subgap Density of States-Based Amorphous Oxide Thin Film Transistor Simulator (DAOTS) for Process Optimization and Circuit Design

Yong Woo Jeon, Sungchul Kim, Sangwon Lee, Dong Myong Kim, and Dae Hwan Kim
School of Electrical Engineering, Kookmin University, Seongbuk-gu, Seoul, Republic of Korea

Sun Il Kim, Sang Wook Kim, Jae Chul Park, U-In Chung, and Chang-Jung Kim
Samsung Advanced Institute of Technology (SAIT), Yongin-si, Gyeonggi-do, Republic of Korea

Je-Hun Lee, Byung Du Ahn, Sei Yong Park, Jun-Hyun Park, Joo Han Kim, and Jaewoo Park
LCD R&D Center, Samsung Electronics, Yongin-si, Gyeonggi-do, Republic of Korea

Abstract
As the oxide TFT-oriented simulator, the subgap density of states-based amorphous oxide TFT simulator (DAOTS) is proposed, implemented, and demonstrated for a-InGaZnO TFTs.
It consists of the parameters having their physical meanings. Moreover, concrete techniques for parameter extraction are supplied. Most preferably, the quantitative self-consistency with experimental data is guaranteed in DAOTS.

1. Introduction
Very recently, amorphous oxide thin film transistors (TFTs) have been emerged as promising building blocks in applications such as flexible active-matrix organic light-emitting diode (AMOLED) displays and large-area high-resolution active-matrix liquid crystal display (AMLCD) backplanes, because they exhibit high field-effect mobilities (μ_{FE}>10 cm^2/Vs) even in the case of room temperature fabrication. Especially, in representative of amorphous oxide TFTs, amorphous Indium-Gallium-Zinc-Oxide (a-IGZO) TFT has many advantages such as high mobility, superior uniformity [1], long-term stability [2], stable chemical bond, and high flexibility resulting from strong ionicity. Moreover, owing to its wide bandgap, a-IGZO is regarded as material adequate for "transparent electronics". Already, several prototype a-IGZO TFT-based circuits for diverse applications have been demonstrated by various companies, which include AM e-papers [3], hard AMOLED displays [4, 5], a flexible AMOLED on stainless steel [6], and the periphery in 3-D stack memories [7]. Furthermore, Ofuji *et al.* have already reported a ring oscillator operation consisting of a-IGZO TFTs at 410 kHz [8], and Yin *et al*. have demonstrated various low voltage digital circuit operations [9].

As the demand for various innovative applications explosively increases, the device model and simulator become more and more indispensable for both the process optimization and the accurate design for maximizing the merits of oxide TFT-based circuits. Considering that the process/structure/layout-dependences of amorphous oxide TFT characteristics cannot be yet fully understood in present, the oxide TFT-oriented model and simulator should have following features, in comparison with the model and simulation works based on commercial technology computer-aided design (TCAD) tools [10-12]:

(1) It must consist of the parameters having their physical meanings (NOT fitting parameters).

(2) The bias-dependence of intrinsic channel mobility (μ_{CH}) must be fully incorporated.

(3) Concrete techniques for parameter extraction have to be supplied.

(4) Most preferably, the quantitative self-consistency with experimental data must be guaranteed.

(5) The process/structure/layout-controlled parameter-dependence should be simply and fast characterized in order to gain a physical insight into the TFT optimization, the degradation mechanism, and the effect to circuit performance.

(6) It has to be easily joinable with various analytical and/or semi-empirical models describing specific device physics and/or reliability issues.

(7) It should be expandable to the circuit simulation.

Motivated by these backgrounds, in this work, the subgap **d**ensity of states (DOS)-based **a**morphous **o**xide **T**FT **s**imulator (DAOTS) is proposed, implemented, and demonstrated for a-IGZO TFTs.

2. DC *I-V* Model based on the 1-D Field Solver
The acceptor-like subgap DOS $g_A(E)$ [eV^{-1}cm^{-3}] of a-IGZO thin film can be experimentally extracted from the optical response of *C-V* characteristic [13-15] or the multi-frequency response of *C-V* characteristic [16] of *n*-channel a-IGZO TFT, for example, which can be modeled as

$$g_A(E) = N_{TA} \times \exp\left(\frac{E - E_C}{kT_{TA}}\right) + N_{DA} \times \exp\left(\frac{E - E_C}{kT_{DA}}\right), \quad (1)$$

where the deep state is assumed to be exponential distribution. If necessary, Gaussian-distributed deep states in $g_A(E)$ can be also easily incorporated into DAOTS. Also, the ionized donor doping concentration (N_D^+) was assumed to be uniformly distributed, which is controlled by the oxygen vacancies (V_O). Here, it should

be noted that if necessary (although it is neglected here for simplicity), the donor-like DOS resulting from V_O ($g_{OV}(E)$) can be also easily incorporated into DAOTS C-language module instead of N_D^+ (it was assumed to be Gaussian-distributed in [11]). In addition, the donor-like DOS ($g_D(E)$) was modeled as

$$g_D(E) = N_{TD} \times \exp\left(\frac{E_V - E}{kT_{TD}}\right) + N_{DD} \times \exp\left(\frac{E_V - E}{kT_{DD}}\right). \quad (2)$$

The flat band voltage (V_{FB}) and the E_{FB} level (defined by the Fermi-level E_F from conduction band minimum (E_C) at V_{GS}=V_{FB} condition) are calculated as follows. Fig. 1(a) shows the energy band diagram (EBD) at V_{GS}=V_{FB} condition. Assuming the gate made of Mo, the V_{FB} is calculated from the electron affinity difference (χ_{Mo}–χ_{IGZO}) and E_{FB} as seen in (3), where it was assumed that the charge density in gate oxide (Q_{ox}) is negligible.

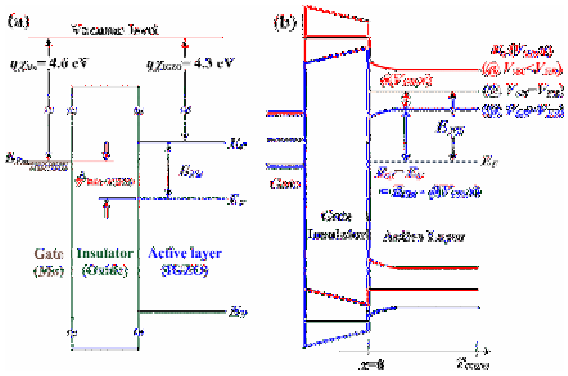

Figure 1. (a) The EBD at V_{GS}=V_{FB} condition and (b) the illustration of V_{GS}-modulated EBD.

$$V_{FB} = \phi_{Mo-IGZO} + \frac{Q_{ox}}{C_{ox}}, \quad \phi_{Mo-IGZO} = q(\chi_{Mo} - \chi_{IGZO}) - E_{FB}. \quad (3)$$

$$\int_{E_V}^{E_C} g_D(E)[1-f(E)]dE - \int_{E_V}^{E_C} g_A(E)f(E)dE - n_{free}(E_F) + N_D^+ = 0 \quad (4)$$

The E_{FB} plays a role of the reference energy level for calculating V_{GS}-modulated potential $\phi(x)$ and energy band as shown in Fig. 1(b). If the N_D, $g_A(E)$, and $g_D(E)$ are given, the E_{FB} can be calculated by (4) with T_{IGZO}=thickness of a-IGZO thin film and $f(E)$=Fermi-Dirac distribution function. Here, the free electron charge density n_{free} is given by

$$n_{free}(x, V_{CH}(y)) = \frac{2}{\sqrt{\pi}} N_C F_{1/2}(\eta_F),$$

$$\eta_F(x, V_{CH}(y)) = \frac{q\phi(x) - E_{FB} + qV_{CH}(y)}{kT} \quad (5)$$

where x=the position along the channel depth direction, y=the position along the channel length direction, $V_{CH}(y)$=the channel potential, and $F_{1/2}$=Fermi-Dirac integral, respectively.

In DAOTS model, the E_{FB} is calculated from $g_A(E)$ and $g_D(E)$ maintaining the consistency between (4) and (5). Fig. 2 shows the relation between E_{FB} and DOS. For instance, the increase of $g_A(E)$ leads to larger E_{FB} for the charge neutrality. Therefore, the E_F level in V_{GS}=V_{FB} condition is the strong function of N_D^+, $g_D(E)$, and $g_A(E)$. Here, the $g_A(E)$ and $g_D(E)$ are designed by controlling the integration process, and the N_D is controlled by adjusting the concentration of oxygen vacancies (*i.e.*, adjusting the O_2 partial pressure in the deposition process of a-IGZO thin film layer).

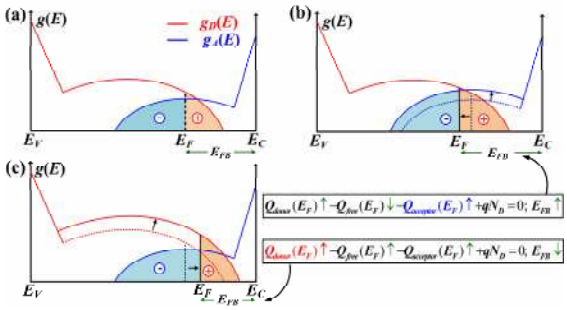

Figure 2. (a) The illustrative relation between E_{FB} and DOS. The increase of (b) $g_A(E)$ or (c) $g_D(E)$ self-consistently changes the initial E_{FB} in DAOTS model.

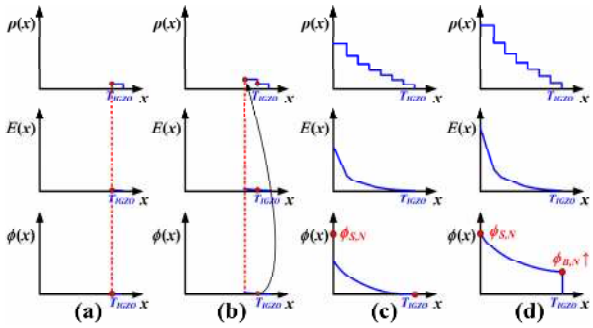

Figure 3. Concept of calculating $\phi(x)$ from the $g_A(E)$ and $g_D(E)$ by using 1-D field solver.

In addition, the 1-D field solver was developed in order to calculate $\phi(x)$ from $g_A(E)$ and $g_D(E)$. The calculation procedure is illustrated in Fig. 3. It is as follows: First, it is presumed that the $g_A(E)$ and $g_D(E)$ are known. Second, in order to derive $\phi_B(\phi_S)$ at a specific surface potential ϕ_S (i.e., $\phi(x=0)$), the back potential ϕ_B (i.e., $\phi(x=T_{IGZO})$) is assumed. Third, a-IGZO thin film is divided into infinitesimal sectors (Δx), and it is assumed that the charge density $\rho(x)$ is constant in a single sector. And then, the $\rho(x=T_{IGZO}-\Delta x)$ is calculated from ϕ_B by using (6)~(8). Fourth, the electric field $E_{IGZO}(x=T_{IGZO}-\Delta x)$ and $\phi(x=T_{IGZO}-\Delta x)$ are calculated by the numerical integration (Fig. 3(a)). Fifth, $\rho(x=T_{IGZO}-2\Delta x)$ is calculated again from $\phi(x=T_{IGZO}-\Delta x)$ by using (6)~(8) (Fig. 3(b)). By iterating this procedure from $x=T_{IGZO}$ to 0, the ϕ_S is gained (Fig. 3(c)). Sixth, unless the calculated ϕ_S agrees with a specific value of ϕ_S, the presumed value of ϕ_B is adjusted and all procedure is iterated until satisfying this agreement (Fig. 3(d)). In this way, the self-consistent $\phi_B(\phi_S)$ is finally acquired.

$$\frac{\partial^2\phi(x)}{\partial x^2} = \frac{q}{\varepsilon_{IGZO}}\left[n_{loc}(x) + n_{free}(x) - N_D^+\right] \quad (6)$$

$$n_{loc}(x, V_{CH}(y)) = \int_{E_V}^{E_C} g_D(E)[1-f(E)]dE - \int_{E_V}^{E_C} g_A(E)f(E)dE \quad (7)$$

$$f(E) = \frac{1}{1 + \exp\left(\frac{E - (E_C - E_{FB} - qV_{CH}(y))}{kT}\right)} \quad (8)$$

Also, the free and localized charge density per unit area (Q_{free} and Q_{loc}) can be calculated from $\phi(x)$, $g_A(E)$ and $g_D(E)$ by using (9) and (10). Thus, by using (11), the self-consistent pair of $\phi_B(\phi_S)$ and $V_{GS}(\phi_S)$ can be solved from the proposed 1-D filed solver. More straightforwardly, the $\phi(x)$ and $E_{IGZO}(x)$ at x=0~T_{IGZO} are determined under a specific solution pair of ϕ_B, ϕ_S and V_{GS}.

$$Q_{free}(x,V_{CH}(y)) = q\int_{x=x}^{x=T_{IGZO}} n_{free}(x,V_{CH}(y))dx = q\int_{x=x}^{x=T_{IGZO}} \frac{2}{\sqrt{\pi}} N_C F_{1/2}(\eta_F)dx\,, \quad (9)$$

$$Q_{loc}(x,V_{CH}(y)) = q\int_{x=x}^{x=T_{IGZO}} n_{loc}(x,V_{CH}(y))dx = q\int_{x=x}^{x=T_{IGZO}} \left[\int_{E_V}^{E_C} g_D(E)[1-f(E)]dE - \int_{E_V}^{E_C} g_A(E)f(E)dE\right]dx\,, \quad (10)$$

$$V_{GS} = V_{FB} + \phi_s + \frac{Q_{LOC}(x=0)+Q_{FREE}(x=0)}{C_{ox}} = V_{FB} + \phi_s + \frac{\varepsilon_{IGZO}E_{IGZO}(x=0)}{C_{ox}}. \quad (11)$$

The V_{GS}-modulated EBD calculated from the proposed 1-D field solver is illustrated in Fig. 4. The V_{GS}-dependent potential along a channel depth direction $\phi(x)$ (including the self-consistent solution pair of ϕ_B, ϕ_S and V_{GS}) is found to be successfully demonstrated. Especially, the floating body effect with ϕ_B is clearly reproduced.

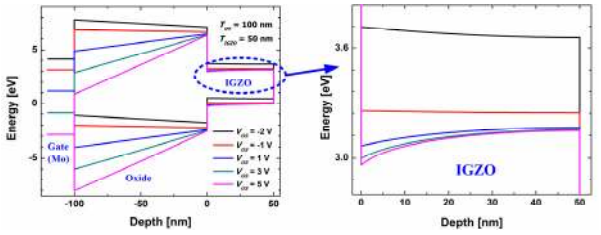

Figure 4. The V_{GS}-dependent EBD calculated from 1-D field solver.

As is the case of a-Si:H TFT, the intrinsic channel mobility μ_{CH} is expressed as the functions of μ_{Band}, Q_{free}, and Q_{loc} as follows:

$$\mu_{CH}(x,V_{CH}(y)) = \mu_{Band} \times \frac{Q_{free}(x,V_{CH}(y))}{Q_{free}(x,V_{CH}(y)) + Q_{loc}(x,V_{CH}(y))}\,, \quad (12)$$

where the Q_{free} and Q_{loc} are the functions of $\phi(x)$, g_A(E) and g_D(E). In order to derive the DC I_{DS}-V_{GS} model, the drift conduction current equation is introduced as

$$I_{DS} = W\frac{dV_{CH}}{dy}\int_{x=0}^{x=T_{IGZO}} \sigma(x,V_{CH}(y))dx,$$

$$I_{DS}dy = W\int_{x=0}^{x=T_{IGZO}} \sigma(x,V_{CH}(y))dxdV_{CH}(y)\,. \quad (13)$$

By integrating (13) from y=0 to y=L with substituting the voltage V_{CH} for the position y in terms of the integral variable, we get

$$I_{DS} = \frac{W}{L}\int_{V_S}^{V_S+V_D}\int_{x=0}^{x=T_{IGZO}} \sigma(x,V_{CH}(y))dxdV_{CH}(y) = q\frac{W}{L}\int_{V_S}^{V_S+V_D}\int_{x=0}^{x=T_{IGZO}} \mu_{CH}(x,V_{CH}(y))\times n_{free}(x,V_{CH}(y))dxdV_{CH}(y). \quad (14)$$

By substituting (12) for the $\mu_{CH}(x, V_{CH})$ in (14), we obtain

$$I_{DS} = q\mu_{Band}\frac{W}{L}\int_{V_S}^{V_S+V_D}\int_{x=0}^{x=T_{IGZO}} \frac{Q_{free}(x,y)}{Q_{free}(x,y)+Q_{loc}(x,y)} \times n_{free}(x,V_{CH}(y))dxdV_{CH}(y). \quad (15)$$

In contrast to single crystalline semiconductor, the μ_{CH} of a-IGZO TFT cannot be out of integral because it is the function of x by itself. By applying Poisson's equation at the interface of a-IGZO/oxide and changing the integration variable from x to $\phi(x)$ (with E_{IGZO}= $-d\phi(x)/dx$), (15) is re-described as

$$I_{DS} = q\mu_{Band}\frac{W}{L}\int_{V_S}^{V_S+V_D}\int_{\phi_S}^{\phi_B} \frac{Q_{free}(\phi,V_{CH}(y))}{Q_{free}(\phi,V_{CH}(y))+Q_{loc}(\phi,V_{CH}(y))} \times n_{free}(\phi,V_{CH}(y))d\phi\left(-\frac{dx}{d\phi}\right)dV_{CH}(y)$$

$$= q\mu_{Band}\frac{W}{L}\int_{V_S}^{V_S+V_D}\int_{\phi_B}^{\phi_S} \frac{q\int_{\phi_B}^{\phi_S}\frac{n_{free}(\phi,V_{CH}(y))}{E_{IGZO}(\phi,V_{CH}(y))}d\phi}{Q_{free}(\phi,V_{CH}(y))+Q_{loc}(\phi,V_{CH}(y))} \times \frac{n_{free}(\phi,V_{CH}(y))}{E_{IGZO}(\phi,V_{CH}(y))}d\phi\,dV_{CH}(y)\,. \quad (16)$$

It is noticeable that the I_{DS}-V_{GS} model in (16) is expressed only as the function of ϕ_S, ϕ_B, V_{GS}, and V_{DS}. Then, thanks to the solution pair of ϕ_B, ϕ_S and V_{GS} from the 1-D field solver, the DC I-V model is consequently the function of V_{GS} and V_{DS}. Here, it should be reminded again that the input parameters of the I-V model in (16) are NOT fitting parameters BUT physical parameters such as μ_{Band}, $g_A(E)$, $g_D(E)$, N_C, N_D, V_{FB}, and E_{FB}. More straightforwardly, the $\mu_{CH}(x, V_{CH}(y))$ in (12) can be used for gaining the average V_{GS}-dependent field-effect mobility (around the source) $\mu_{FE}(V_{GS}, V_{CH}$=0, y=0)=$\mu_{FE}(V_{GS})$=$\mu_{FE}(\phi_S, \phi_B)$ as seen in (17). In addition, in DAOTS model, the influence of S/D parasitic resistance R_S on μ_{FE} is neglected because the characterized a-IGZO TFT has a long channel length (L=30 μm). The R_S-effect will be investigated more in-depth as further studies.

$$\mu_{FE}(V_{GS}) = \mu_{CH}(\phi_S,\phi_B) = \mu_{Band}\frac{q\int_{\phi_B}^{\phi_S}\frac{n_{free}(\phi,V_{CH}=0)}{E_{IGZO}(\phi,V_{CH}=0)}d\phi}{Q_{free}(V_{CH}=0)+Q_{loc}(V_{CH}=0)}\,. \quad (17)$$

3. Parameter Extraction and Device Simulation

Fig. 5 shows the methodology for the parameter-extracting procedure in DAOTS. The effective DOS (N_C) and the band mobility (μ_{Band}) in E_C can be conceptually extracted from the carrier density n_{Hall} and μ_{Hall} in Hall measurement [17]. Also, in this work, $g_A(E)$ was extracted from the same with [16] Then, only the $g_D(E)$ and N_D are pre-assumed as appropriate values and will be finally acquired in the way how they are adjusted with numerical iteration until satisfying the self-consistency between the calculated I_{DS}-V_{GS} and μ_{CH} model and the measured I_{DS}-V_{GS} and μ_{FE} characteristics because they are not yet able to be extracted from the experimental technique. Thus, the fundamental inputs (N_C, μ_{Band}, $g_A(E)$, $g_D(E)$, and N_D) are accepted with various geometrical parameters (such as W, L, T_{IGZO} and T_{ox}) (Fig. 5(a)). Starting from all physical parameters, the V_{FB} and E_{FB} are calculated by using (3)~(4) (Fig. 5(b)). Then, the self-consistent solution pair of ϕ_B, ϕ_S and V_{GS} is acquired by the 1-D field solver and (11) (Fig. 5(c)). Then, the calculation of $I_{DS}(V_{GS}, V_{DS})$ and $\mu_{FE}(V_{GS})$ is completed by using (16)~(17) and compared with the measured I_{DS}-V_{GS} and μ_{FE}-V_{GS} characteristics (Fig. 5(d)). Until the calculated $I_{DS}(V_{GS}, V_{DS})$ and $\mu_{FE}(V_{GS})$ models agree well with the measured ones, the $g_D(E)$ and N_D are adjusted by numerical iterations (Fig. 5(e)). This agreement just is accomplished, like the proposed methodology, and now all of the physical parameters are completely extracted (Fig. 5(f)).

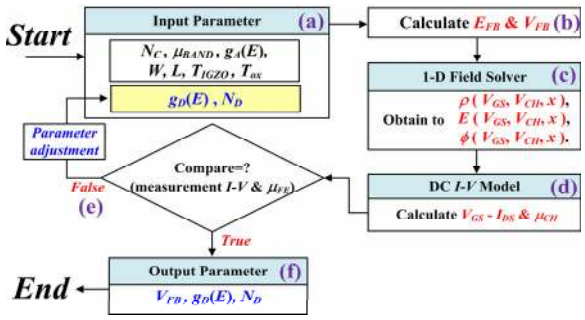

Figure 5. The methodologies for the parameter-extracting procedure and the device simulation in DAOTS.

Here, it is noticeable that in our parameter-extracting procedure, the quantitative self-consistency with experimental data is automatically guaranteed. At the same time, if the $g_D(E)$ and N_D can be experimentally extracted like $g_A(E)$, the methodology in Fig. 5 becomes also very strong tool for the device simulator satisfying desirable features enumerated in Introduction. In addition, the proposed DAOTS plays a significant role of TFT process/structure optimization, because all of N_C, μ_{Band}, $g_A(E)$, $g_D(E)$, and N_D are the process-controlled parameters.

Table I. Finally extracted parameters by using the procedure in Fig. 5.

Parameter	Value	Parameter	Value	Parameter	Value
N_{TA} [$eV^{-1}cm^{-3}$]	8×10^{18}	N_{TD} [$eV^{-1}cm^{-3}$]	1×10^{20}	N_C [cm^{-3}]	6×10^{18}
kT_{TA} [eV]	0.067	kT_{TD} [eV]	0.06	μ_{Band} [cm^2/Vs]	23.5
N_{DA} [$eV^{-1}cm^{-3}$]	5×10^{16}	N_{DD} [$eV^{-1}cm^{-3}$]	1×10^{18}	N_D [cm^{-3}]	5×10^{16}
kT_{DA} [eV]	0.8	kT_{DD} [eV]	0.55	V_{FB} [V]	0.13

4. Results and Discussions

Finally extracted parameters are summarized in Table I. The geometrical parameters are as follows: W/L=50/30 μm, T_{ox}=100 nm, and T_{IGZO}=50 nm, respectively. More noticeably, the $I_{DS}(V_{GS},V_{DS})$ and $\mu_{FE}(V_{GS})$ calculated by DAOTS are compared with the measured ones in Fig. 6(a)~(d). Our results verify that the physical parameter set, which is extracted by means of the proposed methodology, and the implemented DAOTS model can successfully reproduce the measured I_{DS}-V_{GS} and μ_{FE}-V_{GS} characteristics even including the subthreshold region. Especially, a good agreement between the measured $\mu_{FE}(V_{GS})$ and the calculated one from DAOTS implies that the R_S is negligible compared with the channel resistance.

5. Conclusions

As the oxide TFT-oriented simulator, the DAOTS is proposed, implemented, and demonstrated for a-IGZO TFTs. It consists of the parameters having their physical meanings (NOT fitting parameters). Moreover, concrete techniques for parameter extraction are supplied. Most preferably, the quantitative self-consistency with experimental data is guaranteed in DAOTS.

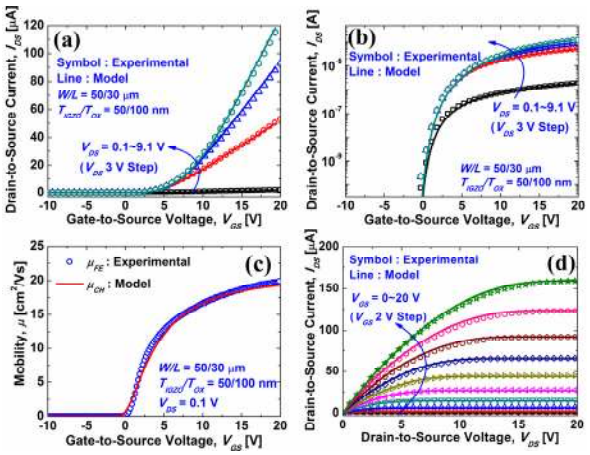

Figure 6. The measured (a) I_{DS}-V_{GS} curve in linear scale, (b) I_{DS}-V_{GS} curve in log scale, (c) $\mu_{FE}(V_{GS})$, and (d) I_{DS}-V_{DS} curve are compared with the results from DAOTS.

If the models of R_S-effect, interface trap density (D_{it}), and parasitic AC capacitance are incorporated into it as further study, the DAOTS is expected to play a significant role of the process optimization and circuit design for innovative oxide TFT-based applications such as display backplane, wearable computers, paper displays, transparent display, solar cell, and 3-D stacked memories. In addition, it is easily joinable with various analytical and/or semi-empirical models describing specific device physics and/or reliability issues, and expandable to the circuit simulation, in comparison with commercial TCAD model.

6. Acknowledgements

This work was supported by the Korea Science and Engineering Foundation (KOSEF) grant funded by the Korea government (MEST) (No. 2009-0080344).

7. References

[1] K. Nomura *et al*., *Nature*, vol. 432, pp. 488-492, 2004.
[2] C. J. Kim *et al*., *IEDM Tech. Dig*., pp. 1-4, 2006.
[3] M. Ito *et al*., *Proc. Int. Display Workshop*, pp. 845-845, 2005.
[4] H. N. Lee *et al*., *Proc. Int. Display Workshop*, pp. 663-663, 2006.
[5] J. K. Jeong *et al*., *SID'08 Dig.*, pp. 1-4, 2008.
[6] M. C. Sung *et al*., *Proc. Int. Meeting on Inf. Display 07 Dig.*, pp. 133-197, 2007.
[7] M.-J. Lee *et al*., *Advanced Functional Materials*, vol. 19, pp. 1587-1593, 2009.
[8] M. Ofuji *et al*., *IEEE Electron Dev. Lett*., vol. 28, pp. 273-275, 2007.
[9] H. Yin *et al*., *IEDM Tech. Dig*., pp. 199-202, 2009.
[10] H.-H. Hsieh *et al*., *SID'08 Dig*., pp. 1277-1280, 2008.
[11] T.-C. Fung *et al*., *J. Appl. Phys*., vol. 106, p. 084511, 2009.
[12] H. Godo *et al*., *SID'09 Dig*., pp. 1110-1112, 2009.
[13] K-C. Jeon *et al*., *Appl. Phys. Lett*., vol. 93, p. 182102, 2008.
[14] J-H. Park *et al*., *IEEE Electron Dev. Lett*., vol. 29, pp.1292-1295, 2008.
[15] J-H. Park *et al*., *IEEE Electron Dev. Lett*., vol. 30, pp. 1069-1071, 2009.
[16] S-W. Lee *et al*., *IEEE Electron Dev. Lett.*, vol. 31, pp. 231-233, 2009.
[17] P. Barquinha *et al*., *IEEE Trans. Electron Devices*, vol. 55, pp. 954-960, 2008.